[redacted]

[redacted]

NACA

RESEARCH MEMORANDUM

PERFORMANCE OF A SWEPT LEADING EDGE ROTOR OF THE SUPERSONIC TYPE WITH MIXED FLOW

By Arthur W. Goldstein and Ralph L. Schacht

Lewis Flight Propulsion Laboratory
Cleveland, Ohio

[redacted]

NATIONAL ADVISORY COMMITTEE
FOR AERONAUTICS

WASHINGTON
January 30, 1953

[redacted]

[redacted]

NATIONAL ADVISORY COMMITTEE FOR AERONAUTICS

RESEARCH MEMORANDUM

PERFORMANCE OF A SWEPT LEADING EDGE ROTOR OF THE SUPERSONIC TYPE WITH MIXED FLOW

By Arthur W. Goldstein and Ralph L. Schacht

SUMMARY

An experimental investigation with Freon-12 as the working fluid was made of a 14-inch-diameter supersonic mixed-flow axial-discharge rotor of the impulse type. The whole series of tests was made twice - once with a set of guide vanes that underturned the air and gave a somewhat lower relative inlet velocity than the design value, and once with a set that gave approximately the design values for velocity and direction. At the design tip speed of 686 feet per second (equivalent value for air, 1564 ft/sec), the weight flow was about 43.5 pounds per second (equivalent air value, 23.7 lb/sec), the pressure ratio was 6.25, and the efficiency was 80.4 percent with the first set of guide vanes. With the second set the figures are 43.3 pounds per second, 6.6, and 78.0 percent. The leading edges of the blades were sufficiently swept to give subsonic velocities normal to the leading edge and in the plane of the blade surface. This permitted large variations of weight flow but did not permit shock surfaces to be formed on the leading edge. Work output was adequately equalized at the discharge end. High tip losses indicated that tip loading and axial length are critical factors. Inadequacy of the axisymmetric design system or blade-to-blade two-dimensional flow analysis is indicated.

INTRODUCTION

The supersonic compressor offers the possibility of high mass flow and pressure ratio with relatively few components, but presents new problems, many of which as yet have no answers. It is shown in reference 1 that large turnings can be efficiently accomplished. Typical remaining problems are the establishment of flow with the desired pressure wave configuration, stability of such configurations, choking of flow because of boundary-layer growth while diffusion occurs near sonic conditions, and discontinuous changes in operating conditions of the compressors.

When compared with the subsonic rotor type, which operates with supersonic shocks in the diffuser, the shockless supersonic rotor (references 2 and 3) appears to be of greater significance because higher mass flow is attainable with higher gas velocities. A comparison with shock-in-rotor types (references 2 and 4) indicates that for high pressure ratios, the strong shocks required are best handled in stationary diffusers where more elaborate techniques of efficiently diffusing the gas may be employed. (Diffusion at high Mach numbers presents difficulties in swallowing the shock and yet obtaining a small enough throat for small losses in the nozzle shock.)

The present paper presents the results of an experimental study made at the NACA Lewis laboratory of the first of two impellers of the shockless type which are identical except that the weight flow of the first impeller was reduced by use of a larger hub diameter. The purpose of this exploratory study is to obtain the operating characteristics of the rotor and to note any problems which may arise, as well as specifically (1) to check the axisymmetric solution (reference 5) by comparing the static pressures at the rotor case with those computed and those to be measured later with the full-flow machine, (2) to determine whether or not the blade sweep causes any difference in the operating characteristics of the impeller, (3) by comparison of the exit flow of the present machine with that to be obtained from the rotor of lower radius ratio to find whether the higher diffusion rates on the full-flow machine will cause a deterioration of the flow over the hub, (4) to ascertain whether the work output of the rotor can be successfully equalized by the method of sweeping back the blade root and gradually unloading the blade, and (5) to determine the operating states of this kind of rotor.

ROTOR DESIGN

The rotor is designed to operate at an isentropic pressure of about 8.0, an equivalent tip speed of 1564 feet per second (686 ft/sec in Freon-12), and an axial Mach number of about 0.85. The initial flow is nonradial with counterrotation, the internal flow is shockless, and the relative discharge flow is nearly axial. Subsonic leading edges are obtained by sweeping the tip back for subsonic normal gas velocities. Work output is equalized at the exit by sweeping the trailing edges back at the root to provide extra blade surface for work input.

The general process of design used consisted of the following steps:

(1) Assumption of rotative speed and inflow and outflow conditions

(2) Assumption of velocity distribution on the blade surfaces at the tip

(3) Assumption of number of blades and calculation of shape of blade contour at the tip. For radial blade elements this establishes the blade shape.

(4) Calculation of effect of blade blockage of flow area for adjustment of blade shapes and flow velocity

(5) Assumption of degree of sweep at leading edge and calculation of shape of swept portion of blade

(6) Calculation of exit region of blade which equalizes work output and unloads blades

(7) Calculation of hub shape according to reference 5

(8) Allowance on the hub for losses or boundary-layer growth to attain the desired velocity distribution

Throughout these computations, the properties of Freon-12 (dichlorodifluoromethane, a commercial refrigerant) were approximated by assuming the gas constant value for Freon and by taking the ratio of specific heats as 1.125.

The inflow velocity distribution was set up on the assumption of a free vortex having constant axial velocity (axial Mach number 0.85 at the tip) and zero radial flow component. The assumption of a small relative rotational velocity at the discharge and the isentropic pressure ratio of 8.0 determined the work input. Therefore when the rotative tip speed (686 ft/sec) was assumed, the inlet rotational velocity at the tip and the entire velocity distribution there were obtained. Assumption of constant work output and zero radial velocity component for the exit flow then determined a free-vortex flow at the exit. The resulting tip conditions are tabulated for Freon-12 at 100° F.

	Tip conditions	
	Entrance	Exit
Absolute velocity at tip, ft/sec	444.2	1129
Relative gas velocity at tip, ft/sec	950	950
Local sonic speed, ft/sec	496.4	496.4
Absolute flow angle	-18° 8'	32° 20'
Relative flow angle	-63° 36'	-5° 56'
Wheel speed, ft/sec	713	

The leading edge of the blade was swept back 45° in the meridional projection (fig. 1) so that the velocity component normal to the leading edge was nearly constant at 0.77 of sonic speed, making it impossible for the leading edge of the blades at the inlet to support a shock wave. When the sweep has been established, the conditions of radial blade elements and free-vortex flow into the blades determine the blade shape completely in the region ABH (fig. 1).

It is shown in reference 5 that when the gas enters the impeller there is a change of velocity, flow direction, and gas state which may be estimated from the blade thickness and orientation. For blades with radial line elements, the blade setting angles are estimated from the assumed conditions upstream of the blades and the assumption of zero radial velocity inside as well as outside the blade region. For these conditions the equations of reference 5 reduce to

$$A\left(1 + \frac{V^2}{2h}\sin^2 \nu\right)^{\frac{1}{\gamma-1}} (\cos \nu - \sin \nu \tan \alpha) \cos \nu = 1$$

(to be solved for ν)

$$V_i = V \cos \nu$$

$$u_i = V_i \sin (\alpha + \nu)$$

$$w_i = V_i \cos (\alpha + \nu)$$

where

A ratio of flow area inside blade region to that outside (projections on a plane normal to axis of rotation)

w_i axial component of gas velocity, ft/sec

α_i $\tan^{-1} u_i/w_i$, deg

ν $\alpha_i - \alpha$ (incidence), deg

h specific enthalpy, (ft-lb)/lb

γ ratio of specific heats

No subscript indicates blade-free region; subscript i, the blade region. (A complete list of symbols is given in the appendix.) The

direction of the blade camber line at the leading edge is set equal to the computed direction of flow inside the blades. The angle of incidence ν is therefore the angle between the blade camber line and the upstream flow direction. As a result of this calculation, there is obtained the solution

Radius (in.)	Angle of incidence ν (deg)	$\frac{u_i - u}{V}$	$\frac{V_i^2 - V^2}{V^2}$
7.0	3.9	0.034	-0.0046
6.0	4.6	.044	-.0065
5.0	5.7	.059	-.0099

Thus the blades are actually set to give two-dimensional flow ($v = v_i = 0$) and turning through an angle of from 3.9° to 5.7°. This angle of attack coupled with the decrease in velocity results in a leading-edge deflection in which approximately 3.7 percent of the work output is accomplished. The change in kinetic energy of the gas is small and corresponds to a change in pressure of about 0.1 percent.

At the blade tip, a velocity distribution was assumed such that the arithmetic average of the pressure and suction surface velocities was a constant. From a small initial loading the suction surface velocity rose to a value of 1120 feet per second at 10 percent of the total arc length of the camber line and maintained this value until 90 percent of the camber line, at which point the value was decreased to the mean value of 950 feet per second by a parabola with zero slope at the end. This velocity distribution was estimated from reference 6 to provide reasonable diffusion rates. To find the blade shape, first solve for the rotational velocity component from

$$\frac{\partial u}{\partial s} = \frac{2}{t} (V_s - V)$$

(see reference 5 for derivation)

where

u rotational velocity component, ft/sec

s arc length along camber line, ft

t distance between suction and pressure surface measured in direction of rotation, ft

V_s relative velocity on suction surface, ft/sec

V relative mean velocity between blades, ft/sec

Here t was determined by assuming 22 blades, made of 1/8 inch thick sheet metal, having an outside diameter of 14 inches. If this equation is integrated for u, then u/V is the sine of the angle between the machine axis and the blade. The axial depth at the tip was determined to be 4.68 inches.

The blade region designed thus far (ABCGA, fig. 1) terminates with unequal work into the gas from root to tip (on line CG). The condition of radial blades is discarded at point C where the tip load begins to decrease. The root load is maintained constant until point F, where the work input is the same as that at point C. The blade surface up to a line joining C and F is made of radial elements. The region CDEF is made of nonradial blades and this region is used to relieve the aerodynamic load to zero.

The hub AE is then determined according to the method of reference 5. An allowance is made on the hub for boundary layer; the growth in displacement thickness of the boundary layer was assumed to be 0.02 inch per inch of gas travel on the wetted surfaces. The correction for all the surface was made on the hub. The coordinates of the blade surface and the hub contour which resulted from this design process are given in table I.

Although the type of impeller being studied is capable of high mass flow, the particular rotor studied has a radius ratio at the inlet of 0.71, which limits the flow. The decision to build both rotors (0.71 and 0.5 radius ratios) was made for the following reasons:

(1) The design computations showed a severe pressure rise along the hub of the design with inlet radius ratio of 0.5 and a considerable alleviation of this difficulty with an inlet radius ratio of 0.7. If the diffusion rate is too severe for the 0.5 radius ratio machine, then another value obtained from the 0.7 radius ratio machine would help establish limits for design practice with allowable losses. If diffusion on the hub of the 0.5 radius ratio impeller is so severe as to cause large regions of separated flow inside the rotor, then regardless of reattachment, the internal flow may be choked at less than design mass flow. Therefore if there exists a limit of flow for this type of machine beyond which there is no gain in reducing the inlet radius ratio, the two rotors should help to define it.

(2) If the mean flow is accurately determined by the axisymmetric solution, the pressure distribution on the casing should be the same

for both rotors. Therefore a check of the axisymmetric solution is expected in that comparison between the pressure distribution for the 0.71 and the 0.5 inlet radius ratio impellers will indicate whether deviations of each pressure distribution from the computed are attributable to effects which may or may not be estimated from the axisymmetric solution.

The present paper reports the experimental results from the rotor with inlet radius ratio of 0.71, although in the design process the solution was continued on for lower values of radius ratio. A picture of the rotor is shown in figure 2.

TEST APPARATUS

The test rig installation and measuring stations are shown in figure 3. The impeller was tested with Freon-12 as the working fluid in a closed circuit as shown in figure 4. The compressor was driven by a 3000-horsepower variable-frequency motor through two sets of gears that allowed a maximum speed of 15,000 rpm. In this system, the pressure developed by the compressor was dissipated across the cylindrical discharge throttle at the end of the radial diffuser. The hot gas flowed from the collector through twin cooler assemblies to the entrance tank. The rate of water flow through the coolers was varied to obtain the desired temperature in the entrance tank. The pressure level in the test loop was maintained at the desired point by controlling the amount of Freon-12 in the system. The purification system maintained a concentration of 97 percent or higher of Freon-12. An additional throttle was provided at the inlet (fig. 4) in order to control the pressure level on the coolers.

PROCEDURE AND INSTRUMENTATION

Over-all performance. - The over-all rating of the compressor was obtained as recommended in reference 7 by using the instrumentation in the surge tank and that at stations 3 and 4 (fig. 3). Four taps were used to measure total pressure and four single-shielded thermocouples (instrument a, fig. 5) were used to obtain total temperature in the surge tank.

At station 3 (about 2.5 in. downstream of impeller blades) six pads 60° apart were provided. Six cone probes (instrument c) or six claw probes (instrument d) were used at this station for measuring total pressure and angle. They were arranged at area centers of three equal annular areas. Static taps on the sides of the cones or the two side tubes on the claws were utilized to set the correct direction.

The static pressure was determined by interpolating the data which were obtained from six taps on the inner wall and six taps on the outer wall.

At station 4 (about 8 in. downstream of impeller blades) six double-shielded thermocouples (instrument e) set at area centers of six equal annulus area were used to obtain total temperature. These probes were set at a fixed angle and were insensitive to angular deviations of the flow encountered.

Surveys. - Four pressure taps on each side of the inlet nozzle (fig. 3) were calibrated for weight flow by surveys made at station 1. Three claw probes (instrument b) were used to obtain total pressure and angle. Traverses were made across the passage in steps of 0.2 inch and came to within 0.13 inch of the hub and casing. Eight wall taps were also provided at this station for static pressure; four were on the inside hub and four on the outside casing. These taps were 90° apart.

Surveys of the passage were also made at station 3 with 3 claw or 3 cone probes for total pressure and angle. Three double-shielded thermocouples were used for total temperature. Traverses were made across the passage in steps of 0.2 inch and came to within 0.13 inch of the hub and casing.

The static pressures for all survey work were determined by interpolating the wall-tap data. Static-pressure taps were installed all along the impeller casing and wherever possible on the inside.

The whole series of tests was made twice - once with a set of guide vanes that underturned the air and gave a somewhat lower relative inlet velocity than the design value, and once with a set that gave approximately the design values for velocity and direction.

Calculations. - In calculating the derived quantities from the measured data, the tables of Freon properties given in reference 8 were used where possible. However, this could not be used directly in correcting the total-pressure instrument readings for the normal shock loss or for computing sonic velocities. The shock losses on the pressure probes were computed from the formula for a gas with constant specific heats using the ratio $\gamma = c_p/c_v$ for the average temperature of the process. Mach numbers were similarly computed using ratios of static to total pressures, although velocities were computed directly from enthalpy differences obtained from the source tables.

Accuracy of data. - Analysis of the data obtained from the exit at the design speed showed the existence of the following circumferential variations in the flow parameters:

Probable error	Pressure (percent)	Angle (deg)	Temperature (°F)
Reading	2	0.9	3.1
Circumferential average	1	.4	1.4

RESULTS AND DISCUSSION

Over-All Performance Characteristics

At the design tip speed of 686 feet per second (equivalent value for air, 1564 ft/sec), the weight flow was about 43.5 pounds per second (equivalent air value, 23.7 lb/sec), the pressure ratio was 6.25, and the efficiency was 80.4 percent with the first set of guide vanes. With the second set the figures are 43.4 pounds per second, 6.6, and 78.0 percent.

A noteworthy feature of the performance of the impeller is the large range of gas flow possible without encountering surge (fig. 6). At 50 percent of normal speed the ratio of maximum to minimum mass flow is almost 2, and at full speed there is a range of 30 percent. The second distinguishing feature is the large rise in available pressure at the high flow rather than the low flow end (see fig. 6). (It will later be shown that the high pressure ratio results from operation with no shock in the rotor, whereas at all other points there is shock compression in the rotor. Several run numbers are given in fig. 6 for subsequent reference.) The rise in pressure ratio occurs at a speed as low as 60 percent of design value, and at design speed the increase is from 4.0 to 6.5. These features contrast with the operation curves of rotors with shock and no sweep which are without the range in mass flow or the sudden rise in stagnation pressure. (Compare, for example, performance characteristics of reference 3.) Sweeping of the blades is therefore believed to be responsible for the large variation in mass flow because the back pressure effect is permitted to leak past the leading edge.

The enthalpy rise is equivalent to the work input to the gas and is shown in figure 7. There is a large rise in work output as the impeller changes to impulse operation, so that the pressure ratio increases because of the work increase and also because of the reduced losses with shockless operation. It will be shown later that this rise in work output is due principally to an increase in velocity at the blade roots where the blades are turned forward, whereas at the tip a slight decrease in velocity occurs and the blades there are directed slightly backward. Higher work output from the impeller with normal guide vanes is a consequence of more initial counterrotation and larger impeller torque.

The striking aspect of the efficiency curves is the fact that when the rotor changes from shock to impulse (shock-free) mode of operation, there is a rise in efficiency of from 10 to 20 points. This is not caused by the removal of a strong shock from the internal flow field as will be demonstrated later, since no strong shocks exist at the high mass flow condition with shock in the rotor. It must therefore be construed as resulting from more efficient flow over the blades and hub when the weak compression shocks are removed.

Entrance Flow

The low velocity guide vanes gave underturning of from 3.5° to 4.0°. Because the entrance flow was so nearly critical, the weight flow was nearly the same as for the normal set, even with a large discrepancy in the value of velocity and a change in absolute angle of flow of about 6.5°. As mentioned previously, the mechanism of establishing the flow is not understood, but the data from both sets of guide vanes make it clear that the shape of the surface of the impeller blades at the entrance is the decisive factor, because the tests with both guide vanes showed the same angle of incidence (approximately 8°) with respect to the impeller blades even though the absolute angle changed 6.5° and the relative Mach number changed 0.1 (fig. 8). The measured angle of incidence is approximately 3° greater than the estimate made on the basis of zero radial velocity in the blades. The variation of the relative flow angle is also shown in figure 8. Comparison of the curves at impulse operation with normal guide vanes for 80 percent, 90 percent, and 100 percent of design speed shows a decrease in angle of attack with increase in Mach number for shockless rotor operation - exactly opposite to expectations from two-dimensional wave pattern analysis. This indicates the inadequacy of two-dimensional analysis for blades with swept leading edges. To clarify this point of the two-dimensional flow patterns, consider a supersonic relative flow with subsonic axial velocity and some blade camber. The effect of the suction surface is extended through characteristics which travel upstream. There is a limiting position beyond which all characteristics are caught in the channel as are all characteristics emanating from the pressure surface. Since the blades cannot exert any torque or tangential momentum change upstream, the net effect of all the characteristics escaping upstream from the limiting position is zero. Hence, the compression and expansion waves cancel each other and set a flow direction upstream at some direction corresponding to a kind of average direction for the suction surface in the upstream influencing region. As the Mach number is increased, the direction of the characteristics is more nearly parallel to the cascade axis and the limiting position moves upstream, so that the direction of the influencing region and therefore the upstream flow more nearly approach that of the leading edge. The angle of attack of

the two-dimensional cascade with cambered blades may thus be expected to increase with Mach number.

Internal Pressure Patterns

Inside the impeller, the only indication available for the state of the gas is the pressure distribution on the casing. These data are shown in figure 9.

The relative flow direction at 6.9 inch radius is -66.2° from the axial direction, and the Mach number is about 1.8. The equations for the blockage effect in the gas induction process with these values and $v_i = v = 0$ give a flow direction inside the blades of -62.8°, and for the velocities

$$\frac{V_i}{V} = 0.9982 \qquad \frac{w_i}{w} = 1.132 \qquad \frac{u_i - u}{V} = 0.02737$$

Therefore, about 2.5 percent of the work output is accomplished at the entrance, and further, a negligible pressure change occurs in the process. Inside the blades the gas must be deflected to the blade direction (about -59.4°), which increases the flow area and increases the Mach number from 1.8 to 1.9.

This increases the relative tangential velocity and subtracts 1.3 percent of the total work input thus leaving a net of 1.4 percent work input accomplished in the induction process. Further, the increase in Mach number decreases the static pressure in the ratio of 0.84. Comparison with the data of figure 9 shows that this pressure drop is about correct, and implies that the flow induction process is very efficient. In the design process, a value of blade angle of -59.4° was postulated for smooth inflow and the estimated flow direction was then estimated to be -63.4°. The discrepancy of 2.8° is not explicable either by the axisymmetric analysis or the two-dimensional blade analysis, although the result of this discrepancy on pressure change is a relatively simple matter to estimate.

After the initial pressure drop there is a pressure rise, a fall, and then a sharp rise and fall. The second wave is shown on a single tap and its existence is questionable. The second wave is reflected from the casing to the hub and then back to the casing and therefore reappears downstream.

To support this contention, figure 9 shows an outline of the hub and the calculated characteristic lines obtained in the design process. These characteristic lines represent curves along which the influence

of conditions at a particular point are propagated and felt elsewhere in the flow field. If (fig. 9(b)) the pressure wave between $z = 2.25$ and $z = 3.5$ is traced along the characteristics to the hub and its reflection, back to the tip, it is clear that the wave for $5.25 < z < 6.75$ is merely a reflection. The same general pattern is seen in figure 9(a). Because the Mach numbers are lower than design, the pattern has a slightly smaller period.

For operation at other than impulse condition, figure 9(a) for the underturned blades shows two distinct states of internal flow. Run 106 is a state of operation obtained when a higher back pressure than that for impulse operation is imposed on the impeller and the weight flow is unchanged. The compression begins at the leading edge; it was impossible to obtain a shock configuration beginning at some other point in the impeller. That the pressure rise consists of weak compressions is supported by two facts: In the first place, the pressure rise is divided into two parts; one wave extends from $z = 2.25$ to $z = 3.75$, and the second extends from $z = 4.8$ to $z = 6.0$. Comparison with the period of pressure waves for run 101 (fig. 9(a)) shows that the second pressure rise is a reflection of the first off the hub. Such a reflection process is possible only with weak waves. These waves are efficient, but could cause a deterioration of the flow over the blade and hub surfaces and a large drop in efficiency. Another reason for suspecting oblique waves is the pressure rise itself in each of the waves; the value is too small for normal shock, although thickening of the boundary layer before shock and subsequent reexpansion would reduce the rate of pressure rise in a similar manner. This process is probably occurring in the second wave in such a manner as to reduce the discharge relative velocity to a subsonic value.

The curve for run 107 is different in several respects. In the first place the pressure exterior to the blades has been affected and the weight flow reduced. This requires subsonic flow in the compressor so close to the leading edge that some of this subsonic flow field can affect the flow upstream of the impeller and the weight flow. This is the mechanism by which the weight flow can be adjusted and steady flow retained. Other differences between the two curves are the greater initial rate of pressure rise in the impeller and the absence of any pressure pattern which would suggest a reflected pressure wave. These two factors confirm the hypothesis of strong shock. The rate of pressure rise is not great enough for a normal shock, however, unless reacceleration is assumed to take place. A normal shock would be inclined about 31° to the axis since the flow would be about 59° to the axis. The blade spacing is about 2 inches, so that the axial depth of the shock is about 0.88 inch. The pressure ratio for Mach number 1.73 would be

$$1 + \frac{2\gamma}{\gamma+1}(M^2 - 1) = 1 + \frac{2(9/8)}{(9/8)+1}(1.73^2 - 1) = 3.11$$

hence, the initial rate of pressure rise would be

$$0.83 \times \frac{3.11 - 1}{0.88} p_{t,0} = 2\ p_{t,0}/\text{inch}$$

The measured value is only 0.72 $p_{t,0}$ per inch. Consequently, either reacceleration and separation must be taking place, or a strong oblique shock exists at the entrance.

Exit Flow

Work distribution. - The work output from the impeller was surveyed very close to the impeller for only the underturning set of guide vanes and the results are shown in figure 10 plotted in the form of enthalpy rise equivalent for an inlet at normal temperature. For impulse operation, the work is nearly uniform, which indicates the success of the method used for equalizing the work input to the gas by sweeping the blades at the exit. When the shock is forced into the rotor, the work is no longer uniform. The reduced relative velocity causes the blade tips to do more work because the blades are directed backward at a slight angle; whereas at the blade roots, the forward turning causes a substantial reduction in work output. On the average, the change of the guide vanes causes a change in the whirl component of flow at the inlet, and this causes a difference in work output which checks the change in inlet whirl.

Pressure output. - The distribution of total pressure at the exit is plotted in figure 10 and shows that all the losses are concentrated at the tip because for the condition of uniform work output at the exit, the lower stagnation pressure at the tip implies an increased entropy over the value at the root. This is not an indication that the losses occurred there, but subsequent discussion will show that this is probably the case. In the present design the blade-to-blade average velocity was to be constant at the tip and conservative surface velocities chosen; whereas at the root, the average channel velocities turned out to have high initial diffusion followed by expansion.

If large losses resulted from this process, it is quite possible that these losses would not show up at the root because of the relative rotation of the gas inside the flow channels. Consequently, the exit total pressure data are not decisive for determining the efficiency of the flow over the hub.

Velocity vector. - The discharge angles relative to the impeller are shown in figure 11 and indicate fair agreement for the underturned set of guide vanes. For the normal guide vanes the agreement is not so good in that overturning of 3° occurred at the tip and 7° at the root. The blades were designed to point in the direction of flow with the loading to diminish to zero at the trailing edge; it is therefore difficult to see how overturning could occur unless the axial velocity changes downstream of the blades. This anomaly indicates the possibility of instrument error.

The relative Mach number (fig. 11) is somewhat lower than design value at the root and very much lower at the tip. To attain design value on the average, a greater allowance could be made for boundary-layer growth. The data indicate that about 18 percent of the exit area should have been allowed instead of 6 percent. However, a more efficient internal flow process would improve this situation somewhat.

Impeller and casing torque. - Average values of work input to the gas are compared with the moment of momentum change of the gas and indicate rather high friction on the casing. If Q_r is the torque exerted by the impeller and Q_c that exerted by the casing, the net torque on the gas imparts a rate of moment of momentum given by

$$Q_r - Q_c = \left[(rc_\theta)_3 - (rc_\theta)_1\right] W$$

where

r radial distance from axis of rotation

c_θ whirl component of the gas velocity

W flow rate of gas, lb/sec

The moment of momentum increment is a mass integrated average. The work input of the impeller is ωQ_r, where ω is the angular velocity of the rotor, and goes into the energy rise of the gas

$$W\Delta H = \omega Q_r = \omega Q_c + W\omega\Delta(rc_\theta)$$

The discrepancy

$$\Delta H - \omega\Delta(rc_\theta) = \frac{\omega Q_c}{W}$$

is therefore a result of friction at the casing. Furthermore, as a result of drag of the casing on the gas, the blades exert more torque on the gas, and consequently, the casing friction may be expected to increase the work input to the gas over the design value.

With the underturned set of guide vanes, there is a design value of $\Delta H/\sqrt{\theta}$ = 19.9 Btu per pound, a measured average value of about 21.7 (temperature indication), a wattmeter indicated value of 21.8, and $\omega\Delta(rc_\theta)$ = 19.3 Btu per pound. The frictional effect in this rotor is quite large, amounting to

$$\frac{21.7 - 19.3}{21.7} 100 = 11.1 \text{ percent}$$

2611

At 90 percent speed a 10 percent discrepancy also exists. For measurements with the normal guide vanes the discrepancies are 6.4 percent at full speed and 6.9 percent at 90 percent full speed. (A reduction is to be expected because of the larger counterrotation and consequent larger frictional turning of the gas in the direction of impeller rotation.) This large discrepancy was checked further to establish reliability. Since the wattmeter checked the temperature rise, this component of the calculation is believed to be correct. The weight flow computed from the inlet survey at 100 percent speed and impulse operation is 43.9 pounds per second and the exit survey gives 44.7 pounds per second. At 90 percent speed the figures are 40.6 and 40.9. With the normal guide vanes the weight flow figures are 43.0 and 43.0 for full speed and 41.0 and 41.5 for 90 percent of full speed. In the Mach number range of the tests, an assumed error in static pressure of 10 percent results in a weight flow error of 4 percent and a velocity error of -4 percent. The weight flow measurements indicate that the accuracy of the velocity and angle measurements is satisfactory. The figures showing a discrepancy are therefore considered reliable.

If these figures are reliable, then somewhat the same effect should be obtained in turbine data where large rotational velocities exist. Data were taken from a turbine chosen at random; the main factor in the selection was the availability of the data. The turbine is a 14-inch cold-air turbine of NACA design with 44 rotor blades. At design point the pressure ratio was 1.8 and the efficiency was 89 percent. The rotational component of the absolute gas velocity at the rotor tip was 0.645. The work output discrepancy here was found to be 13 percent, even though the rotational gas velocity was about one-half the value for the compressor.

Rotor Losses

A rough estimate will be made of the rotor losses in order to determine relative magnitudes and to obtain some hints as to the most desirable modifications to make in the design assumptions.

Surface friction. - The allowance for growth of the displacement thickness of the boundary layer is 0.020 inch per inch of flow. If

this boundary layer is assumed distributed throughout the fluid, the corresponding energy loss is 3 percent of the input. An estimate of the loss in a smooth pipe of the same hydraulic radius as the flow channel gives exactly the same result. Because of the welded construction of the impeller, a loss of about 7 percent would perhaps be a more reasonable figure for surface friction losses estimated from channel flow.

Friction with the casing is large. If the frictional force in the rotational direction is assumed proportional to the absolute rotational velocity of the gas and the resultant force is equal to the tangential component multiplied by c/c_θ, then the frictional force may be computed. With c and c_θ assumed to vary linearly through the compressor, the power loss may be estimated. On this basis, the estimated loss turns out to be 28 percent for the data with underturning guide vanes and 17 percent for the normal guide vanes. If to this is added 3/4 the loss for steel pipe friction (to avoid counting friction on the case twice), there result computed efficiencies of 67 percent and 78 percent for the two cases. These numbers are not accurate (although the second figure does agree with the data (fig. 7) by some coincidence), but they do indicate that the greater part of the loss can be attributed to friction at the casing.

Distribution of low-energy gas at exit. - Examination of the exit total-pressure distribution and Mach number distribution (figs. 10 and 11) shows that greater losses occur at the tip but also appear to be distributed through the fluid to some extent. The pressure ratio at the root indicates nearly isentropic flow in that region and therefore the blade shape appears highly efficient. Distribution throughout the fluid of losses occurring at the blade tips may normally be expected because of the counterrotation of the gas in the channels resulting from the relative negative whirl which is a consequence of irrotationality of the gas and of the wheel rotation. The order of magnitude of this rotation may be estimated by setting

$$\varphi = \omega T$$

where

φ rotation angle of gas in a particular channel between blades

ω wheel velocity

T time spent by gas in channel

If V is the average gas velocity and L, the average flow path length,

$$\varphi = \frac{\omega L}{V} = \frac{\omega r}{V}\frac{L}{r}$$

If the design value of relative velocity at the tip is chosen, then from the channel dimensions,

$$\varphi = 40^\circ$$

However, the actual gas velocity at the casing was less than design, and furthermore, the low-energy gas travels more slowly so that although 40° is a reasonable minimum, the actual figure may be in the neighborhood of 80°. This could account for the distribution of losses at the exit.

Implications for design. - The data from this impeller indicate that the efficiency could be improved by the following modifications: The most important problem is the reduction of friction at the casing. Provided other changes do not cause the flow to deteriorate, the full-flow design can be expected to be more efficient than the rotor tested because the same tip losses are expected with a larger weight flow. Other factors which may be expected to reduce this source of loss are the use of shorter wheels by employing more blades of equal solidity and the use of higher rotative speeds to obtain the same work output with less rotation imparted to the gas. Higher speeds with lower blade loadings should reduce both the tip losses and surface diffusion losses and reduce gas velocities relative to the casing. Operation with guide vanes giving more counterrotation shows a smaller frictional torque effect and a substantial reduction in estimated resultant loss. This conclusion is not verified by the measured efficiencies, possibly because of the higher initial blade loading.

SUMMARY OF RESULTS AND CONCLUSIONS

A 14-inch supersonic rotor of high specific mass flow (inlet axial Mach number 0.85) and radius ratio 0.71 at the inlet, designed for impulse operation at the tip and uniform work output, was tested in Freon-12 with a normal set of guide vanes and a set which underturned the gas.

With the normal set of guide vanes, at design tip speed of 686 feet per second the rotor developed a pressure ratio of 6.6 and an efficiency of 78 percent at a weight flow rate of 43.3 pounds per second. With the set which underturned the gas, the pressure ratio was 6.25, the efficiency was 80.4 percent, and the weight flow was 43.5 pounds per second.

The pressure ratio varied moderately and the work input to the gas was nearly constant for a large range of weight flow less than the maximum. At the maximum weight flow two modes of operation were possible: One mode showed the same work input as the low weight flow end and

somewhat lower pressure ratio. The second mode of operation showed a large gain in work input, pressure ratio, and efficiency over the remainder of the curve. The sudden rise in pressure ratio and work with change to shockless operation is attributable to the forward turning of the blades at the root.

The shape of the blades definitely sets the inflow conditions as revealed by comparison of tests with the two guide vanes. The mechanism of inflow with blade sweep is imperfectly understood because the expected measured flow incidence angle was about 3° higher than calculated. (The analysis was based on the assumption of instantaneous adjustment to flow inside the blades with zero radial deflection of the gas.) The analysis by two-dimensional wave theory in surfaces of constant radius is also inadequate since this indicates an increasing angle of attack with Mach number, which is contrary to the data.

The inflow process whereby the gas is induced into the flow channel between the blades is an efficient process, indicating that although the present method of design does not accurately determine the inflow, it does yield an efficient inducer.

Sweep of the leading edge of the rotor blades adds weight flow range to the compressor characteristic by permitting the subsonic flow field to extend upstream of the blades by radial leakage of the pressure.

The blades of this impeller are generally efficient, as indicated by high pressure ratio, except near the tips of the blades. The greater part of the losses appears to originate at the blade tips and therefore most of the effort for improvement should be directed toward reduction of these losses. Efficiency may be increased by the use of a lower radius ratio. Reductions in casing friction might be accomplished by the use of more blades in shorter wheels and of higher rotative speeds.

The tip losses show up distributed at the exit because of rotation of the gas in the blade channels; the rotation of the gas is of the order of 40° to 80°.

A system of pressure waves which bounce back and forth from hub to tip (possibly resulting from the finite blade number) indicates the inadequacy of the two-dimensional blade-to-blade design or the two-dimensional axially symmetric flow assumption. A definitely three-dimensional method or an approximation to one is required for accurate calculation of the pressure wave patterns.

Equalization of the work input from root to tip was successfully accomplished by the method of continuous blade loading at the root for a small section of blading which did not consist of radial blade elements.

Lewis Flight Propulsion Laboratory
National Advisory Committee for Aeronautics
Cleveland, Ohio

APPENDIX - SYMBOLS

The following symbols are used in this report:

A	ratio of flow area inside the blade region to that outside (projections on a plane normal to axis of rotation)
c	absolute velocity of gas
c_θ	whirl component of absolute velocity of gas
ΔH	specific enthalpy rise
h	enthalpy
L	average flow path length
M	absolute Mach number, ratio of absolute fluid velocity to local velocity of sound
M'	relative Mach number, ratio of fluid velocity relative to rotor to local velocity of sound
p_s	static or stream pressure
p_t	absolute total or stagnation pressure
Q_c	torque exerted by casing
Q_r	torque exerted by impeller
r	radial distance from axis of rotation
s	arc length along camber line of blade
T	time spent by the gas in channel
t	distance between suction and pressure surface of two adjacent blades and measured in direction of rotation
u	rotational component of relative gas velocity
V	relative mean velocity of gas between blades
V_s	relative velocity of gas on suction surface
W	flow rate of gas

w axial component of gas velocity

z distance parallel to axis of rotor

α angle between axis of rotation and relative velocity vector

γ ratio of specific heats

δ ratio of actual inlet total pressure to standard sea-level pressure

2611

ϵ angle between axis of rotation and absolute velocity vector

η efficiency of rotor

θ ratio of actual inlet stagnation temperature to standard sea-level temperature

ν $\alpha_1 - \alpha$ (deflection angle)

φ rotation angle of gas in passing through blade channels

ω angular velocity of rotor

Subscripts:

0 entrance tank upstream of nozzle (see fig. 3)

1 rotor entrance (see fig. 3)

3 instrument station 2.5 inches downstream of impeller blade (see fig. 3)

4 instrument station 8 inches downstream of impeller blade (see fig. 3)

e equivalent value for normal temperature and pressure

i indicates the blade region

REFERENCES

1. Liccini, Luke L.: Analytical and Experimental Investigation of 90° Supersonic Turning Passages Suitable for Supersonic Compressors or Turbines. NACA RM L9G07, 1949.

2. Wright, Linwood C., and Klapproth, John F.: Performance of Supersonic Axial-Flow Compressors Based on One-Dimensional Analysis. NACA RM E8L10, 1949.

3. Ullman, Guy N., Hartmann, Melvin J., and Tysl, Edward R.: Experimental Investigation of a 16-Inch Impulse-Type Supersonic-Compressor Rotor. NACA RM E51G19, 1951.

4. Boxer, Emanuel, and Erwin, John R.: Investigation of a Shrouded and an Unshrouded Axial-Flow Supersonic Compressor. NACA RM L50G05, 1950.

5. Goldstein, Arthur W.: Axisymmetric Supersonic Flow in Rotating Impellers. NACA TN 2388, 1951.

6. Goldstein, Arthur W., and Mager, Artur: Attainable Circulation about Airfoils in Cascade. NACA Rep. 953, 1950. (Supersedes NACA TN 1941.)

7. NACA Subcommittee on Compressors: Standard Procedures for Rating and Testing Multistage Axial-Flow Compressors. NACA TN 1138, 1946.

8. Buffington, Ralph M., and Gilkey, W. K.: Thermodynamic Properties of Dichlorodifluoromethane (F-12). A.S.R.E. Circular No. 12, The American Society of Refrigerating Engineers (New York), 1931.

TABLE I - BLADE AND HUB COORDINATES[1]

Axial distance (in.)	Angular coordinate of blade center line (deg)			Hub radius (in.)
	Root	6.457 in. radius	Tip (7.0 in. radius)	
		Radial	Radial	
0	0	---	---	5.022
.477	7.218	---	---	5.030
.977	14.586	---	---	5.079
1.477	21.779		---	5.176
1.977	28.861			5.324
2.477				5.490
2.601	35.742			
2.977				5.650
3.224	40.120			
3.477				5.786
3.848	43.180			
3.977				5.888
4.472	45.350			
4.977				5.974
5.095	46.790			
5.251	47.051			
			Nonradial	
5.477				5.972
5.718			47.646	
5.753	47.636			
5.977				5.960
6.137	47.817			
		Nonradial		
6.185			48.088	
6.254	47.832			
6.477				5.948
6.585		47.845		
6.653			48.491	
6.755	47.638		---	
6.977			---	5.940
7.017	47.387		---	
	Nonradial			
7.033		47.821	---	
7.445	46.865		---	
7.477			---	5.930
7.481		47.788	---	
7.873	46.330	---	---	
7.977		---	---	5.927
8.301	45.796	---	---	5.927

[1]The blade root begins at $z = 0$, becomes nonradial at $z = 7.017$ in., and ends at $z = 8.301$ in. The section at $r = 6.457$ in. begins at $z = 1.435$ in., becomes nonradial at $z = 6.137$ in., and ends at $z = 7.481$ in. The tip section begins at $z = 1.977$ in., becomes nonradial at $z = 5.251$ in., and ends at $z = 6.653$ in.

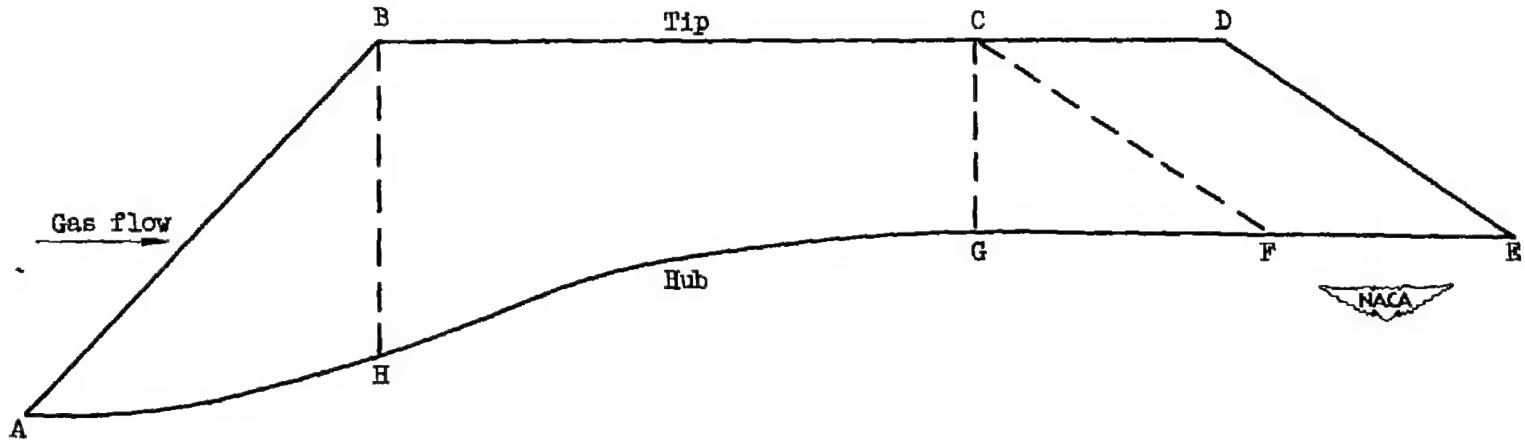

Figure 1. - Regions of blade differentiated in design process.

Figure 2. - 14-inch supersonic axial-discharge mixed-flow compressor rotor.

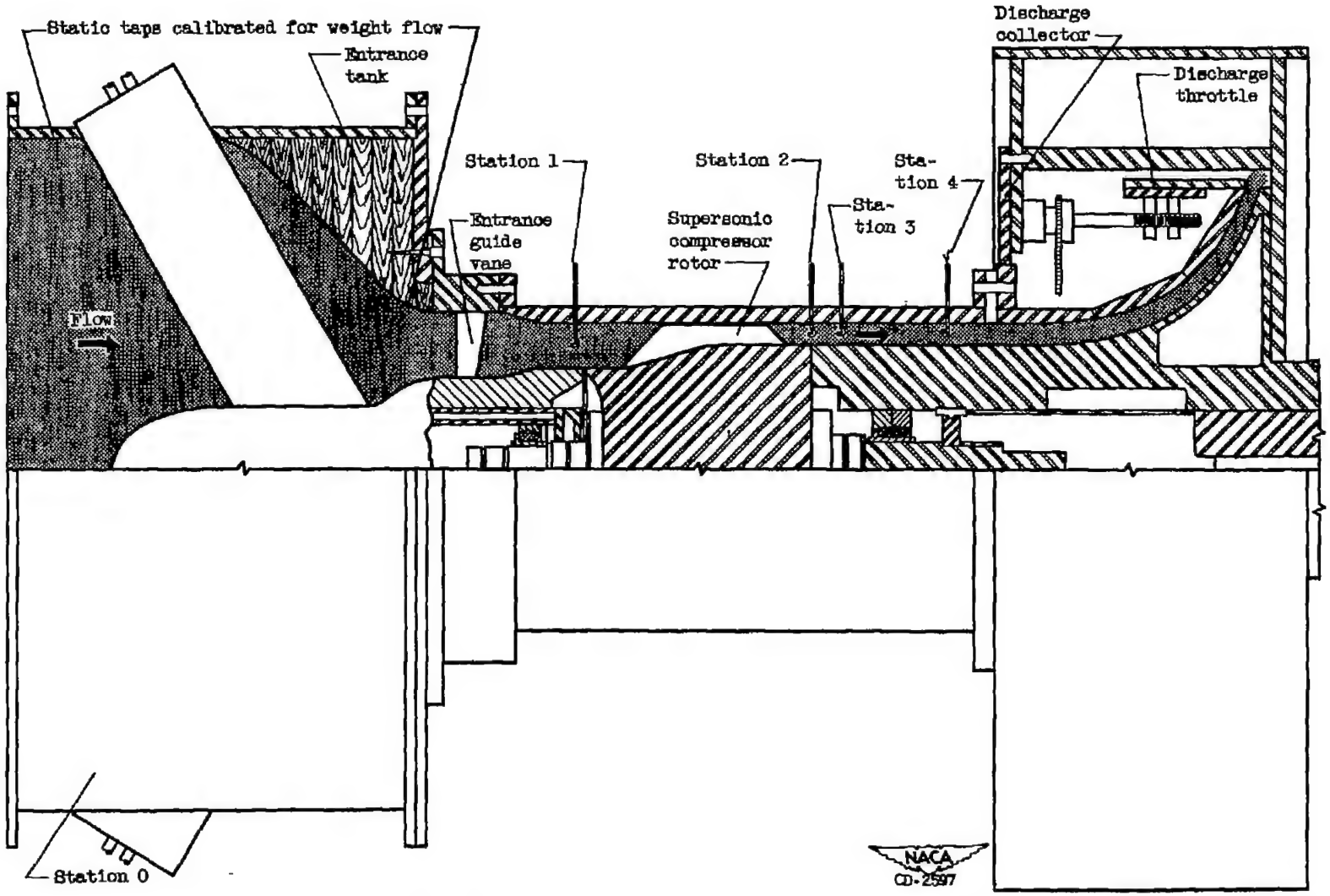

Figure 3. - Schematic diagram of 14-inch supersonic compressor test rig.

Figure 4. - Schematic diagram of piping assembly and compressor installation.

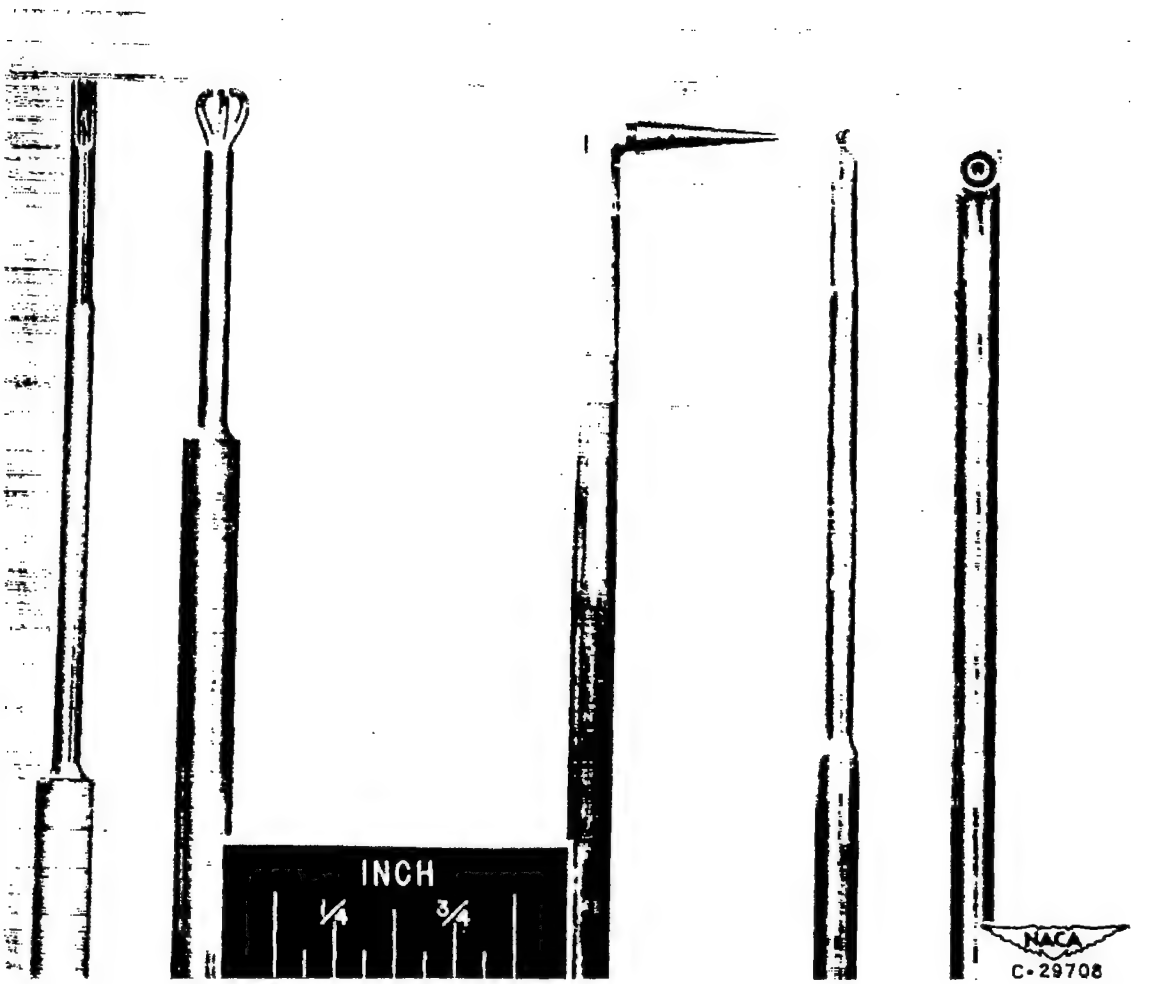

Figure 5. - Instruments used in tests.

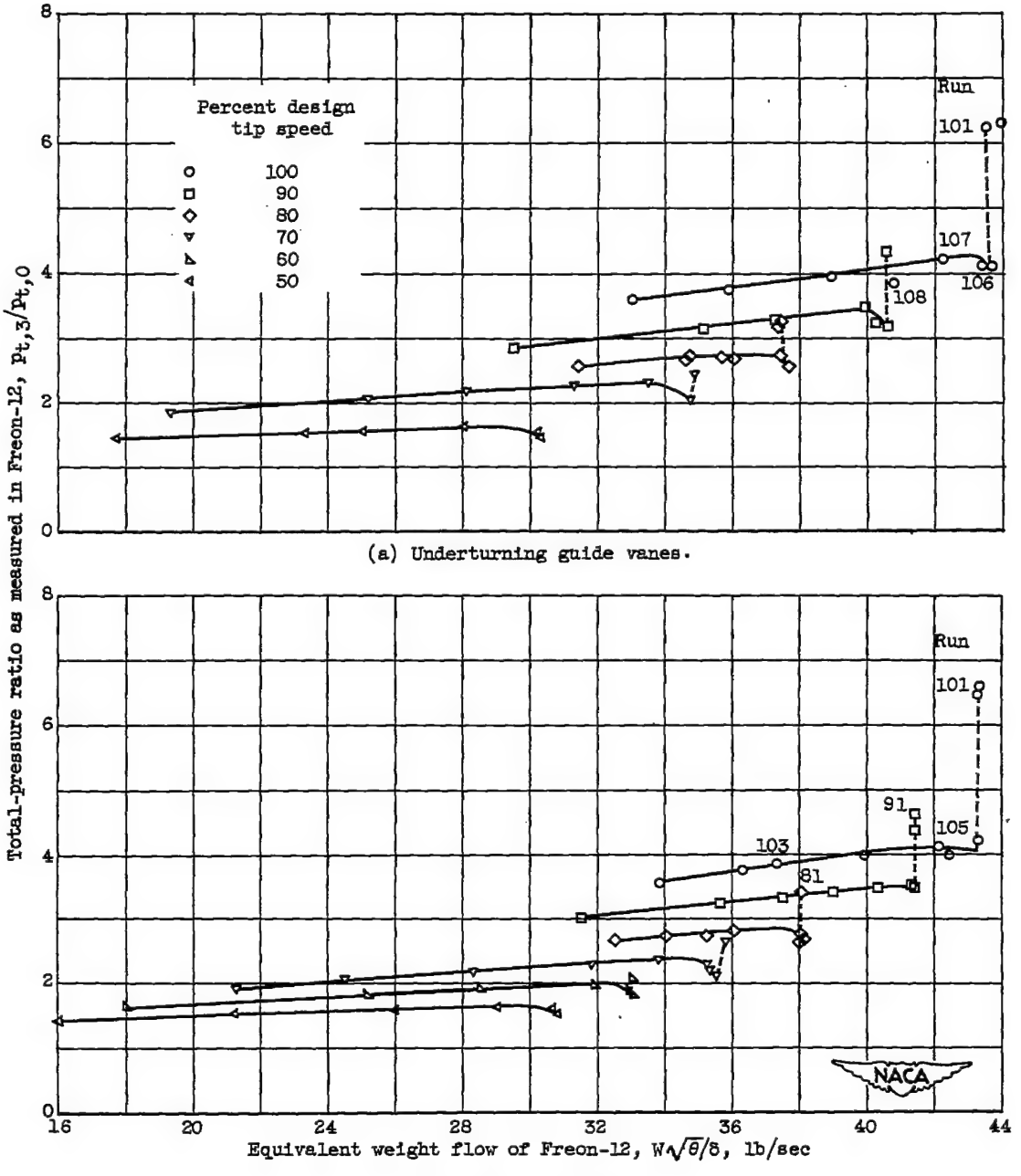

Figure 6. - Performance characteristics for 14-inch supersonic compressor rotor.

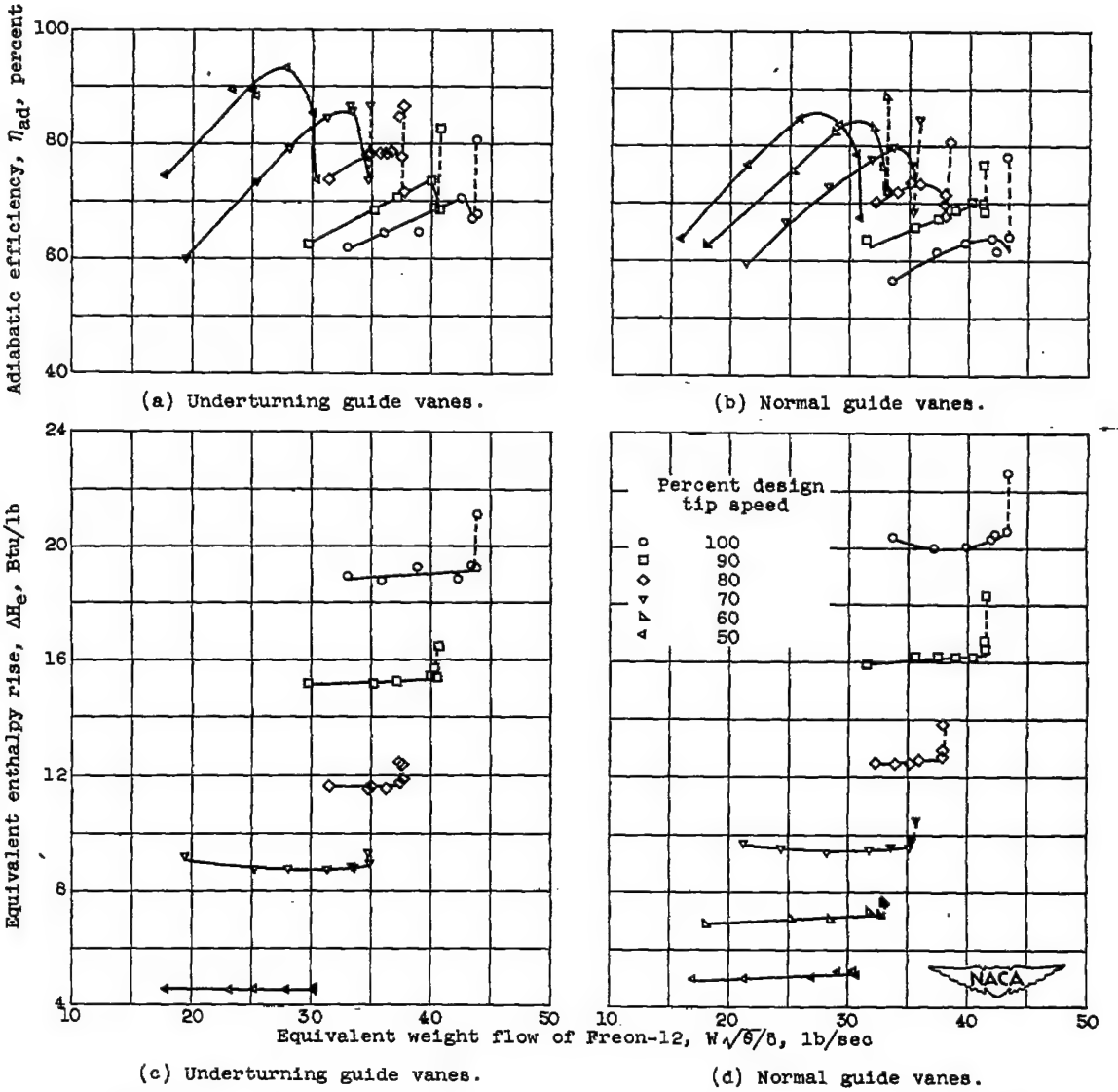

Figure 7. - Performance parameters of 14-inch supersonic compressor rotor at various compressor rotor speeds as measured in Freon-12.

2611

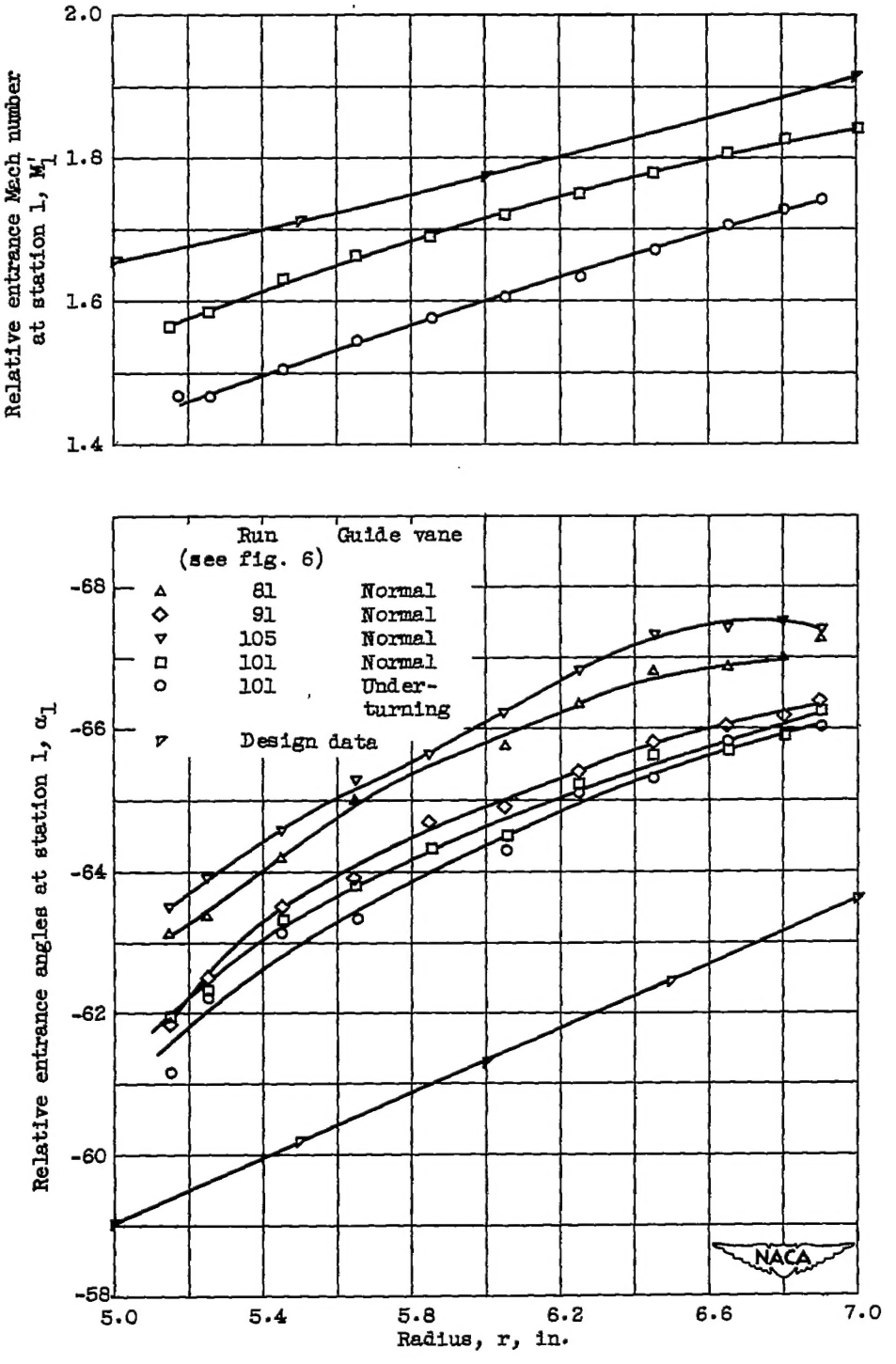

Figure 8. - Conditions (at station 1) upstream of 14-inch supersonic compressor rotor for several operating points as measured in Freon-12.

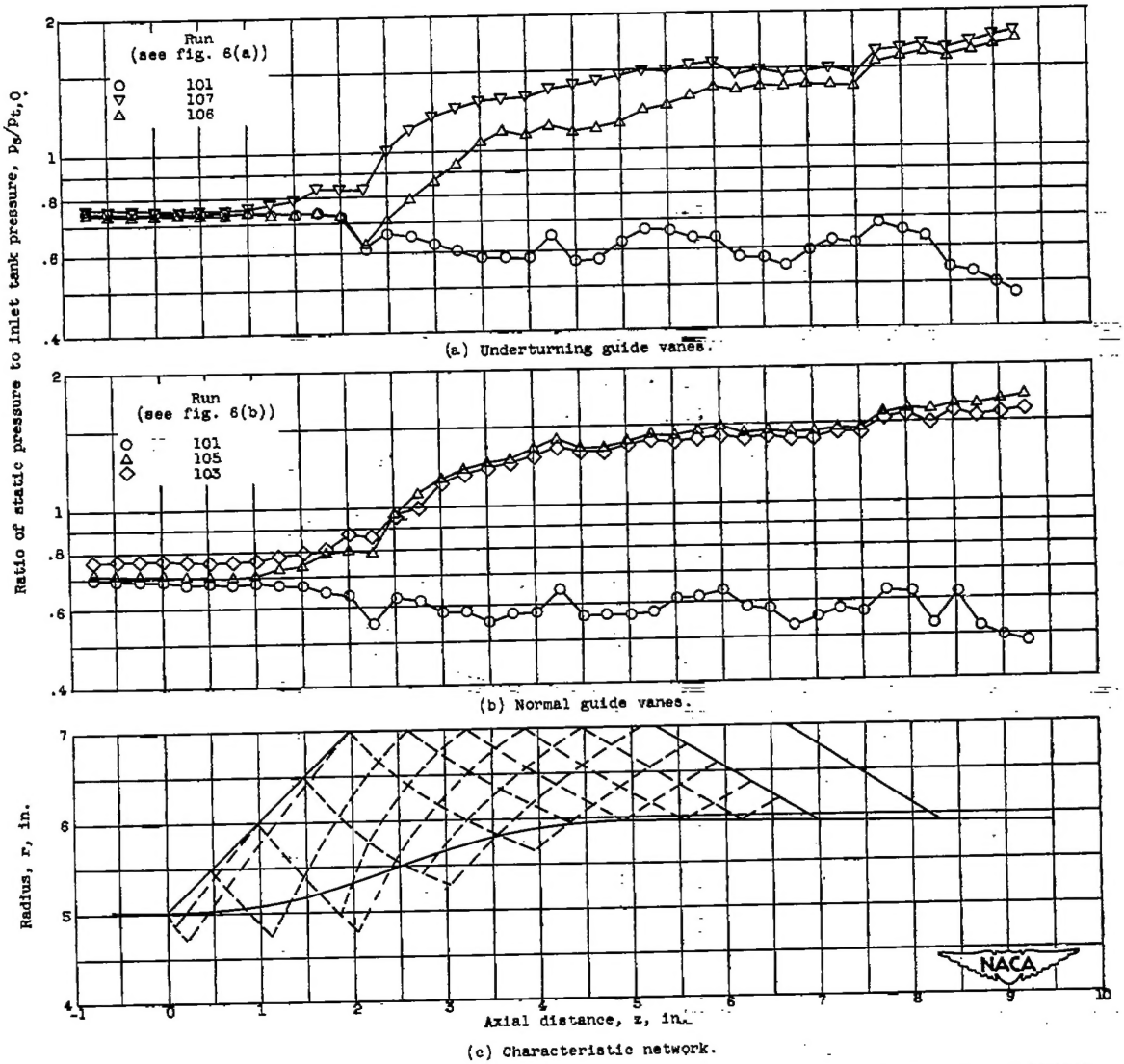

Figure 9. - Sketch of design characteristic network and static-pressure distribution along casing of 14-inch supersonic compressor for 100 percent design equivalent speed and several back pressures.

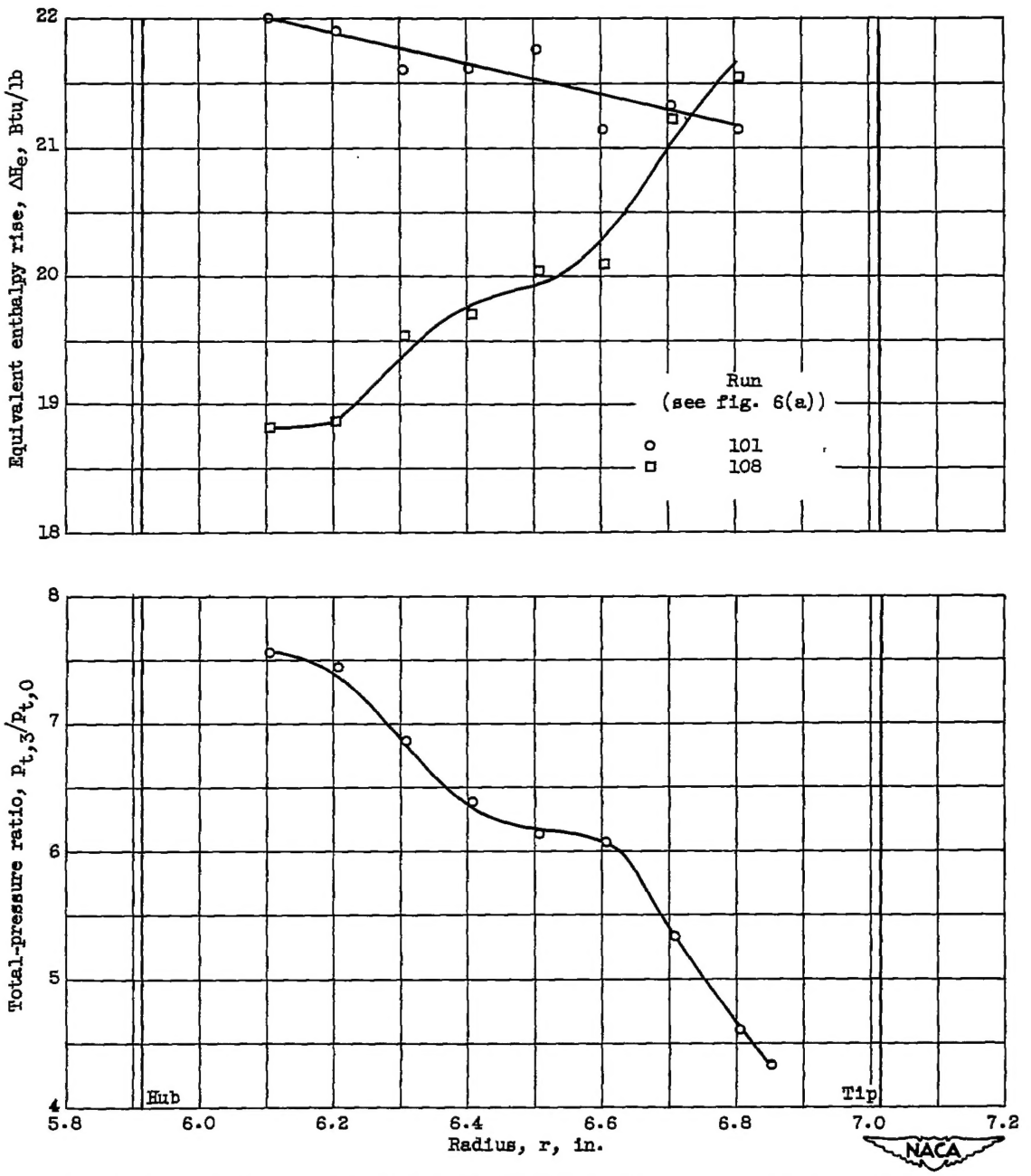

Figure 10. - Conditions (at station 3) downstream of 14-inch supersonic compressor rotor for 100 percent design equivalent rotor speed.

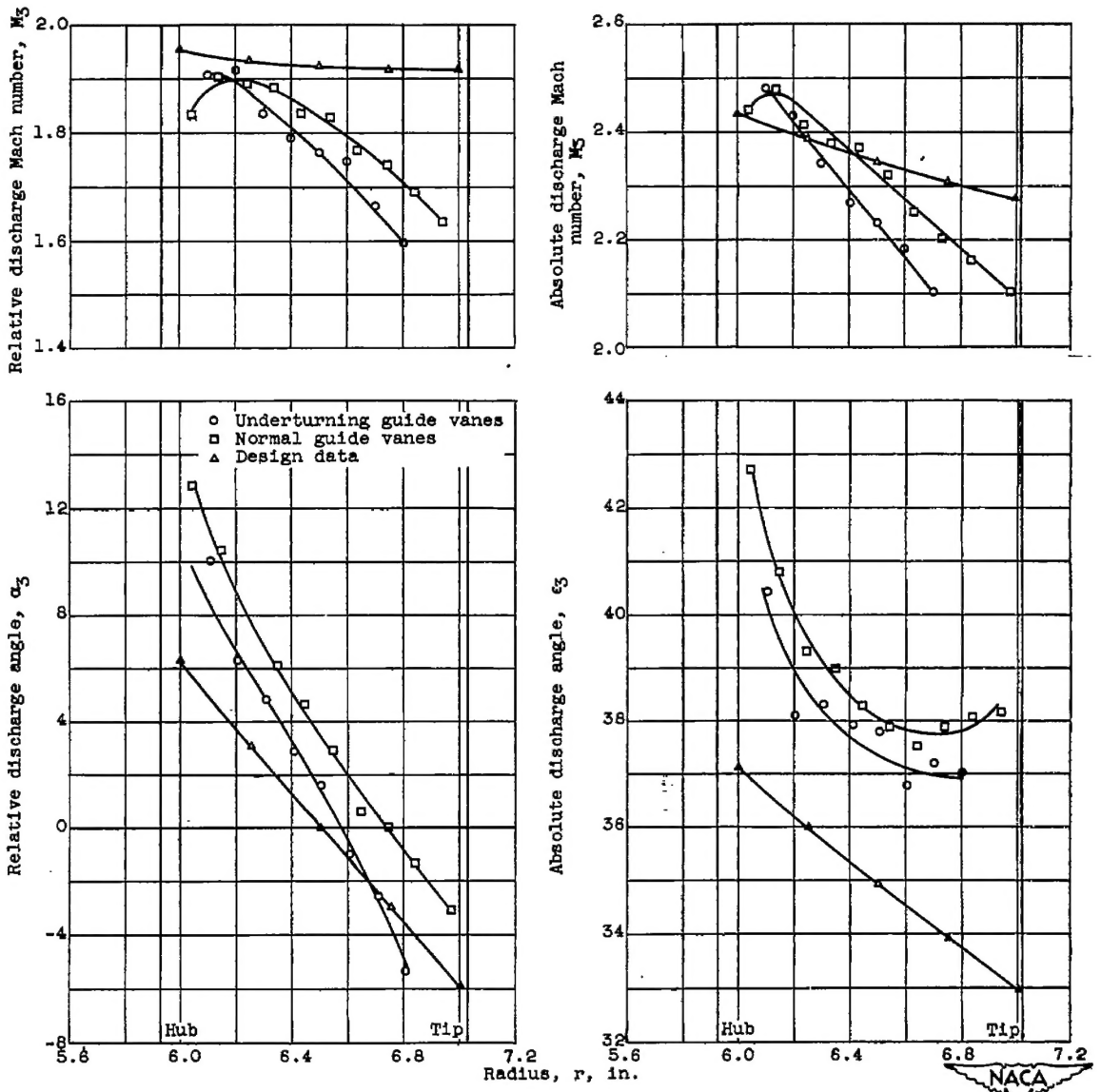

Figure 11. - Conditions (at station 3) downstream of 14-inch supersonic compressor rotor for 100 percent design equivalent rotor speed and maximum pressure ratio as measured in Freon-12.

NACA-Langley - 1-30-53 - 400